# Resonant-Enhanced Spectroscopy of Molecular Rotations with a Scanning Tunneling Microscope

**Fabian Donat Natterer,[†,‡] François Patthey,[†] and Harald Brune[†,*]**

[†]Institute of Condensed Matter Physics (ICMP), École Polytechnique Fédérale de Lausanne (EPFL), Station 3, CH-1015 Lausanne, Switzerland. [‡]Present address: Center for Nanoscale Science and Technology, NIST, Gaithersburg, MD 20899.

**ABSTRACT** We use rotational excitation spectroscopy with a scanning tunneling microscope to investigate the rotational properties of molecular hydrogen and its isotopes physisorbed on the surfaces of graphene and hexagonal boron nitride (*h*-BN), grown on Ni(111), Ru(0001), and Rh(111). The rotational excitation energies are in good agreement with $\Delta J = 2$ transitions of freely spinning *p*-$H_2$ and *o*-$D_2$ molecules. The variations of the spectral line shapes for $H_2$ among the different surfaces can be traced back to a molecular resonance-mediated tunneling mechanism. Our data for $H_2$/*h*-BN/Rh(111) suggest a local intrinsic gating on this surface due to lateral static dipoles. Spectra on a mixed monolayer of $H_2$, HD, and $D_2$ display all three $J = 0 \rightarrow 2$ rotational transitions, irrespective of tip position, thus pointing to a multimolecule excitation, or molecular mobility in the physisorbed close-packed layer.

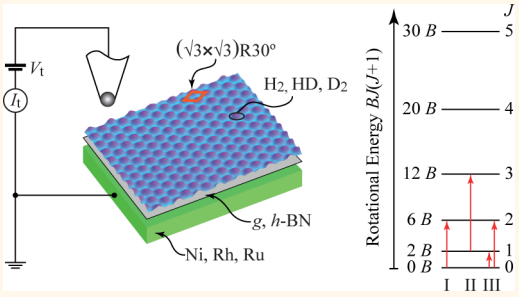


**KEYWORDS:** scanning tunneling microscopy · inelastic electron tunneling spectroscopy · rotational excitation spectroscopy · resonant-enhanced spectroscopy · nuclear spin

Many of the intriguing properties of molecular hydrogen can be traced back to the quantum mechanics of its two alike nuclei. The nucleons are fermions, and the Pauli principle implies the total molecular wave function to be antisymmetric with respect to proton permutation. Since the vibrational and the electronic ($^1\Sigma_g^+$) ground states are symmetric, either the rotational or the nuclear wave functions have to be antisymmetric. Thus, the antisymmetric nuclear singlet state (para) requires a symmetric rotational wave function with even rotational quantum numbers *J*, whereas the symmetric nuclear triplet state (ortho) implies an antisymmetric rotational wave function with odd *J*. Conversion between the two nuclear spin isomers is forbidden by symmetry. Therefore, each of them remains in its rotational subspace of either even or odd *J* states, and knowledge of the rotational state provides information about the nuclear spin state. The rotational states distinguish themselves by their energies $E = BJ(J + 1)$, where $B = \hbar^2/2I$ is the rotational constant and *I* is the molecule's moment of inertia. The existence of nuclear disparate forms of $H_2$ with room temperature equilibrium abundance of 1:3 for para/ortho, has been predicted by Heisenberg.[1] The first preparation of pure para-$H_2$ enabled the confirmation of this prediction by emission spectra and heat conductivity measurements in the gas phase.[2] Note that similar thoughts apply to deuterium and, in more general terms, to any homonuclear diatomic and polyatomic molecule. The *B* values of some representative molecules are listed in Table 1. The spectroscopy of the resulting rotational excitations identifies the molecular chemical and isotope species and their nuclear configuration, and it reveals bond lengths.

Looking at the rotational constants in Table 1 and at the rotational energy ladders of the nuclear disparate species shown in Figure 1, one infers that these energies are for the light molecules readily accessible to inelastic electron tunneling spectroscopy (IETS)[4,5] with a conventional 4 K STM. Nevertheless, the spectroscopy of rotational excitations with STM-IETS was reported only very recently,[6,7] in contrast to the spectroscopy of vibrational[8−10] and magnetic[11−14] excitations dating back 14 and 10 years,

* Address correspondence to harald.brune@epfl.ch.

Received for review April 10, 2014 and accepted July 6, 2014.

**Published online July 07, 2014**
**10.1021/nn501999k**

**TABLE 1. Rotational Constants $B = \hbar^2/2I$ for Selected Diatomic and Polyatomic Molecules with Indistinguishable Nuclei in Their Vibrational and Electronic Ground State[3,a]**

| molecule | $B$ (meV) |
|---|---|
| $H_2$ | 7.36 |
| HD | 5.54 |
| $D_2$ | 3.71 |
| $^{14}N_2$ | 0.247 |
| $^{16}O_2$ | 0.178 |
| $CH_4$ | 0.65/0.65/0.65 |
| $H_2O$ | 3.46/1.80/1.15 |
| $NH_3$ | 1.17/1.17/0.77 |

[a] Polyatomic molecules have rotational constants for different symmetry axes.

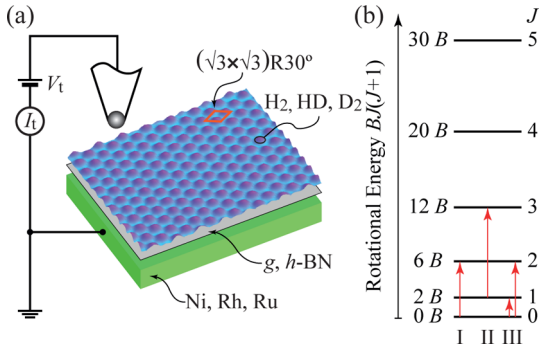


**Figure 1. (a) Schematic of our experiment showing the hydrogen monolayer, physisorbed on either graphene (*g*) or hexagonal boron nitride (*h*-BN), grown on a metallic substrate (Ni, Rh, or Ru). The hydrogen ($\sqrt{3} \times \sqrt{3}$)R30° superstructure is indicated by the lozenge. (b) Rotational level diagram for diatomic rigid rotor, expressed in units of the rotational constant *B*. The diagram is drawn for a population of (I) solely even ($p$-$H_2$, $o$-$D_2$, $o$-$^{14}N_2$), (II) uniquely odd ($o$-$H_2$, $p$-$D_2$, $p$-$^{14}N_2$, $^{16}O_2$), and (III) both rotational levels.**

respectively. The first reason for the late discovery of rotational excitation spectroscopy (RES) with the STM is the difficulty of adsorbing the molecules in a state where they can freely rotate. This issue was solved by adding a spacer layer of hexagonal boron nitride (*h*-BN) promoting physisorbed states that exhibit quasi free 3D rotations.[6] In addition, the *h*-BN spacer created a significantly larger RES signal ($\Delta\sigma/\sigma$)[6] than detected for metal adsorbed molecules.[7] The second reason is that the mechanism of STM-RES is far from being understood. Former studies used neutron diffraction,[15,16] nuclear magnetic resonance,[17,18] high-resolution electron energy loss spectroscopy (HREELS),[19−21] and high-resolution inelastic He atom scattering.[22] HREELS is closest to STM-IETS since in both cases electrons are injected into the molecules and lose the rotational excitation energy. However, HREELS uses 5 eV primary electrons that excite negative-ion resonances, with the rotation being one of the relaxation channels, while in STM-IETS the primary electrons have exactly the kinetic energy of the rotational excitation at the $dI/dV$-conductance step. An ultralow energy collective negative ion resonance state has been proposed[6] implying STM-RES being limited to interacting molecular ensembles.

The aim of the present paper is to establish a better understanding of the actual excitation mechanism and to explore in addition to *h*-BN also graphene as a spacer layer. We present hydrogen and deuterium STM-RES results on graphene (*g*) and *h*-BN grown on Ru(0001), Ni(111), and Rh(111), as illustrated in Figure 1. All systems exhibit the characteristic gas-phase rotational excitation energies showing that the molecules are rigid 3D rotors on any one of these substrates. We detect subtle variations in the spectroscopic signatures between the substrates that are quantitatively reproduced by a theoretical model originally proposed for resonance-enhanced vibrational spectroscopy with the STM.[23,24] This model naturally explains why former STM-RES signatures were fully quenched[25−27] or strongly suppressed[7] when the molecules were directly adsorbed onto a metal substrate. STM-RES on isotopic mixtures of $H_2$, HD, and $D_2$ show conductance steps of all three molecular species independent of the tip position pointing toward collective excitations. Finally, this model suggests external control parameters of the molecular rotations.

## RESULTS AND DISCUSSION

Figure 2 shows STM images of the four investigated $H_2/sp^2$-monolayer/substrate combinations in the upper panels. The interaction between the $sp^2$-monolayers and the substrate is such that strong chemical bonds are formed whenever the C atoms of graphene, respectively, the N atoms of the *h*-BN, are on top of the underlying metal atoms. For any other stacking, the layers are only van der Waals bound. On Ni(111), *g*- and *h*-BN are almost perfectly lattice matched and form strongly bound (1 × 1) structures.[28−31] The corresponding STM images in Figure 2b reveal the $H_2$ ($\sqrt{3} \times \sqrt{3}$)R30° superstructure on a flat background. This superstructure has previously been reported for the surfaces of graphite,[15,17,32] of *h*-BN[33] bulk samples, and on *h*-BN/Ni(111).[6] The molecules reside on the 6-fold coordinated hollow sites.

The other two systems are lattice mismatched and form moiré structures. Graphene has two C atoms per unit cell leading to 2/3 of the moiré period where either one of them is close to a substrate atom on-top site. Consequently, the *g*/Ru(0001)-(23 × 23) structure[34,35] in Figure 2a shows weakly bound moiré hills on a dark connected background. Figure 2c shows that *h*-BN adopts the inverted topography on Rh(111) since only the N atom strongly binds to the underlying Rh *d*-states throughout the moiré periodicity, whereas the B atom's interaction is modulated.[36] Therefore, the *h*-BN/Rh(111)-(12 × 12) unit cell displays well-localized depressions surrounded by a connected higher lying and weakly bound area referred to as wires.[37−39] On both moiré structures, well-ordered $H_2$

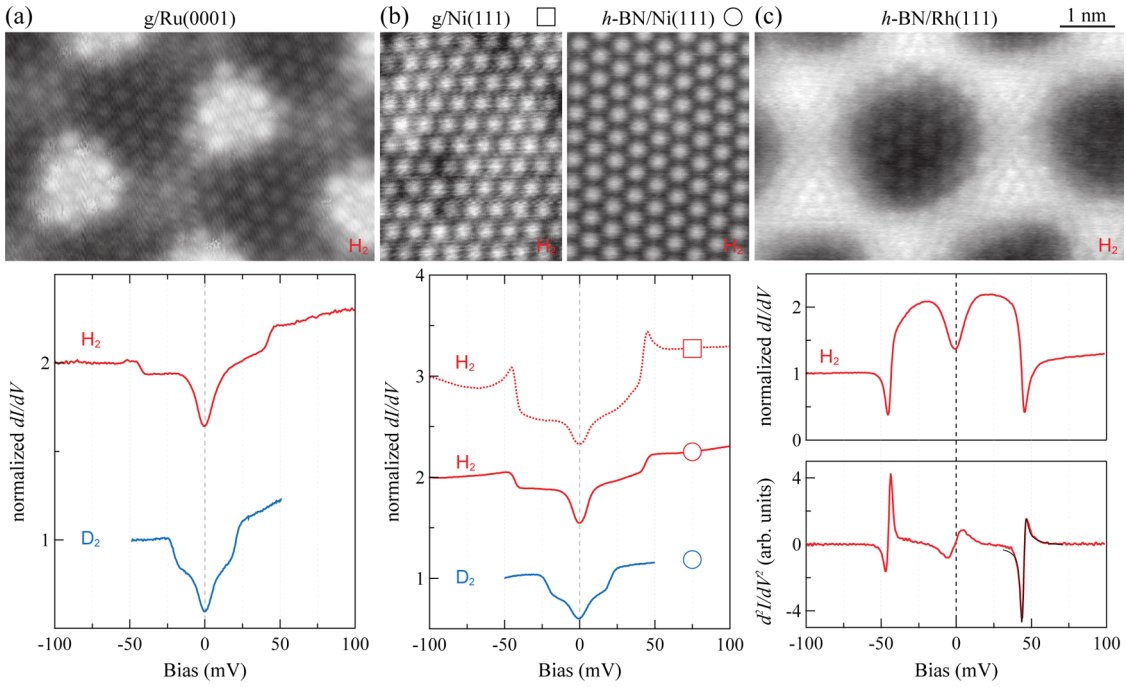


**Figure 2. STM images of hydrogen superstructures on graphene and *h*-BN (top) with the corresponding rotational excitation spectra (bottom). (a) The hydrogen molecules adsorb in the ($\sqrt{3} \times \sqrt{3}$)R30° superstructure in the valleys of the *g*/Ru(0001)-(23 × 23) moiré unit cell. The d*I*/d*V* traces were recorded in their center, and the curves show averages of 201 ($H_2$) and 56 ($D_2$) point spectra. (b) Hydrogen superstructure on *g*/Ni(111)-(1 × 1) (left) and *h*-BN/Ni(111)-(1 × 1) (right). The *dI*/*dV* data represent averages of 156 ($H_2$/*g*, dashed line), 889 ($H_2$/*h*-BN), and 193 ($D_2$/*h*-BN) spectra. (c) Around 20 hydrogen molecules are trapped in the depressions of the *h*-BN/Rh(111)-(12 × 12) unit cell. The *dI*/*dV* curve was recorded in the center of the moiré depressions and represents an average of 289 single spectra. The superimposed fit with eq 1 (black) shows excellent agreement with the measured $d^2I/dV^2$ spectra. [$T_{STM}$ = 4.7 K, (a) $V_t$ = −20 mV, $I_t$ = 50 pA, (b, left) $V_t$ = −50 mV, $I_t$ = 50 pA, (b, -right) $V_t$ = −20 mV, $I_t$ = 20 pA, (c) $V_t$ = −20 mV, $I_t$ = 5 pA. The spectra were recorded with an impedance of 1 GΩ and normalized with respect to the starting conductance. The lowermost spectra in (a) and (b) are drawn to scale, and the others are vertically offset by one unit each for clarity.]**

($\sqrt{3} \times \sqrt{3}$)R30° superstructures are localized in the strongly bound stacking areas.

The lower panels of Figure 2 show the *dI*/*dV* signal of physisorbed hydrogen and deuterium on the four surfaces in the regions of the ($\sqrt{3} \times \sqrt{3}$) superstructure. Irrespective of the underlying substrate, the measured *dI*/*dV* spectra show pairs of large conductance steps at the threshold energies of ±44 meV and ±21 meV for hydrogen and deuterium, respectively. The low-energy excitations (≤5 meV) are ascribed to phonons of the molecular layers[6] and not further discussed in the following. The observed *dI*/*dV* signatures are characteristic of the rotational transitions $J = 0 \rightarrow 2$ of *p*-$H_2$ and *o*-$D_2$ with energies of 6 $B_{H_2}$ = 44.2 meV and 6 $B_{D_2}$ = 22.3 meV, respectively (cf. Figure 1b). Therefore, for each isotope only one spin isomer is present at the surface, the respective other one would have 10 *B* as lowest rotational excitation energy (the absence of the complementary isomers is attributed to a fast conversion of the $J = 1$ to the $J = 0$ nuclear spin isomer of the respective isotope[40,41]). The close coincidence of the measured rotational energies for physisorbed hydrogen with the gas phase values indicates the weak surface−molecule interaction and illustrates how the decoupling layers *g*- and *h*-BN can be used to study intrinsic molecular properties with STM-RES.

A closer analysis of the line shape of the spectra in Figure 2 reveals valuable information about the excitation mechanism. While we observe an increasing differential conductance at the excitation threshold for hydrogen on *g*/Ru(0001), *g*/Ni(111), and *h*-BN/Ni(111), a negative differential resistance (NDR)[42,43] is seen for hydrogen on *h*-BN/Rh(111) which resembles an asymmetric Fano-line shape.[44] Previous STM contributions attributed the NDR for tunneling across adsorbed molecules to a conformational change of the molecule in the junction,[45] or to a two-state switching between two levels with different conductance.[25] Similarly, an asymmetrically coupled two level model[46] was proposed to describe NDR of single molecules in break-junction devices.[47,48] Note, however, that these models consider translational modes rather than the rotational excitations observed in this work.

In the following, we will interpret our observations by a resonance-mediated tunneling process which naturally explains both NDR and stepwise increase in differential conductance at the excitation threshold, as well as all the intermediate cases [such as for $H_2$/*g*/Ni(111) in Figure 2b]. We employ the formalism of Persson and Baratoff,[23,24] considering inelastic electron tunneling *via* molecular resonances. Although the model was originally developed for the excitation of

vibrational modes for chemisorbed molecules, it is safe to also include molecular rotations for a physisorbed molecule in its description provided that the following analogy applies. The model assumes a broad and short-lived resonance that is formed due to strong hybridization of the molecule with the surface. However, a broad resonance state can also exist in form of a negative ion resonance (also referred to as shape resonance)[49,50] for molecules that are only weakly adsorbed on the surface. The incoming electron can then either be temporarily trapped in this broad resonance state of the molecule and relax *via* all available degrees of freedom, for instance by inelastically transferring a vibrational or rotational quantum to the molecule,[51] or the electron can tunnel elastically into the continuum instead. This fundamental relationship is encountered for a wide range of physical processes and emerges from the quantum interference between a discrete set of states with a continuum.

The model of Persson and Baratoff has the position of the molecular resonance ($\varepsilon_a$) with respect to the Fermi energy $E_F$, the resonance width ($\Gamma$), the excitation threshold ($\Omega$), and a coupling parameter ($\delta\varepsilon$) as parameters. The differential conductance ($\sigma$) as a function of the applied voltage ($V_t$) and in proximity of the threshold reads[23,24]

$$\sigma = \frac{(\delta\varepsilon)^2}{(\varepsilon_a+eV_t)^2+(\Gamma/2)^2} \times \left\{ \frac{(\varepsilon_a+eV_t-\Omega)^2-(\Gamma/2)^2}{(\varepsilon_a+eV_t-\Omega)^2+(\Gamma/2)^2}\Theta(eV_t-\Omega) - \frac{\Gamma}{\pi}\frac{\varepsilon_a+eV_t-\Omega}{(\varepsilon_a+eV_t-\Omega)^2+(\Gamma/2)^2}\ln\left|\frac{eV_t-\Omega}{\Delta}\right| \right\} \quad (1)$$

where $e$ refers to the magnitude of the electron charge. From the relationship in eq 1, we can appreciate the natural appearance of NDR whenever $|\varepsilon_a + eV_t - \Omega| < \Gamma/2$.[24] The character of the observed features is therefore a sensitive gauge for the alignment of the molecular resonance with respect to $E_F$ ($V_t = 0$ V).

We approximated the measured spectra by iteratively adjusting the above parameters and by taking thermal and modulation broadening into account.[4,52] We achieved excellent agreement between simulated and experimental $d^2I/dV^2$ spectra with the parameters found in Table 2 and exemplarily displayed for $H_2$/*h*-BN/Rh(111) in Figure 2c and in more detail shown around the rotational threshold for all substrates in Figure 3. The widths $\Gamma$ of the resonances appear to be very large but are in good agreement with typically reported values for shape resonances.[49] The NDR found for $H_2$/*h*-BN/Rh(111) can now be rationalized through a shift of the resonance to $\varepsilon_a = -200$ meV, whereas the resonance position of the other systems is found around +1 eV. The *h*-BN/Rh(111) system is particular, in that the (12 × 12) moiré pattern is

**TABLE 2. Fit Parameters for Simulated $d^2I/dV^2$ Spectra in Figure 2 c and Figure 3 Using eq 1[a]**

| | Ω (meV) | $\varepsilon_a$ (meV) | Γ (meV) | $T_{eff}$ (K) |
|---|---|---|---|---|
| $D_2$/*g*/Ru | 20.8 ± 0.1 | 660 ± 40 | 100 ± 60 | 7.7 ± 0.5 |
| $H_2$/*g*/Ru | 42.8 ± 0.2 | 660 ± 40 | 120 ± 50 | 8.7 ± 0.5 |
| $H_2$/*g*/Ni | 43.0 ± 0.5 | 750 ± 30 | 500 ± 60 | 7.7 ± 0.5 |
| $H_2$/*h*-BN/Ni | 44.1 ± 0.2 | 1200 ± 20 | 310 ± 90 | 10.7 ± 0.5 |
| $D_2$/*h*-BN/Ni | 20.8 ± 0.1 | 1200 ± 80 | 170 ± 100 | 9.7 ± 0.5 |
| $H_2$/*h*-BN/Rh | 44.5 ± 0.1 | −200 ± 20 | 820 ± 40 | 5.0 ± 0.5 |

[a] The parameters Ω, $\varepsilon_a$, and Γ are the rotational excitation threshold, the position of the molecular resonance with respect to $E_F$, and the width (FWHM) of the molecular resonance, respectively. The energy cutoff parameter $\Delta \ll \Gamma$ was set to 1 meV,[24] and the errors were determined by varying the parameters until the disagreement with experimental spectra became significant, with a minimal increase of 20% in the sum of the squared residuals. The last parameter $T_{eff}$ is the effective temperature used to extract the intrinsic widths of the excitation and thereby the lifetime of the rotationally excited state.

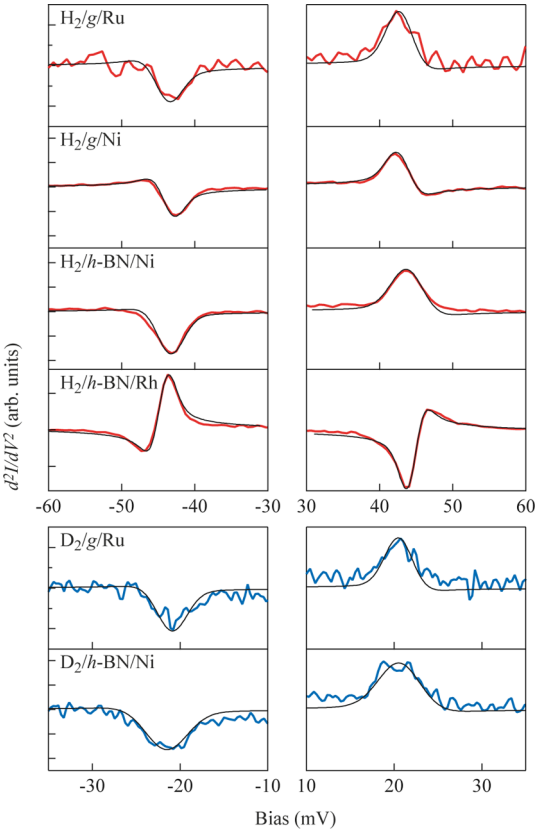


**Figure 3. Experimental $d^2I/dV^2$ data for $H_2$ (red), and for $D_2$ (blue) around the $J = 0 \rightarrow 2$ rotational thresholds with superimposed simulated spectra (black) using eq 1 and the fit parameters of Table 2.**

accompanied by a periodic modulation of the work function between the depressions and the wire structure. These work function modulations entail electrostatic dipole rings[53] that were shown to immobilize molecules and atoms.[37,53,54] We can therefore attribute the shift of the molecular resonance position for $H_2$/*h*-BN/Rh(111) to the local variations of the electrostatic potential on this surface. Consequently, this

system is a prototype for the effect of molecular gating and presents an interesting perspective for further STM-RES studies.

Note that the interplay of the resonance position and the resonance width may lead to a suppression of the rotational excitation. The former could be shifted, for instance, by tuning the sample work function. It appears that an unfortunate alignment or improper width of the resonance may be the reason why earlier contributions missed to report STM-RES for hydrogen on copper and silver[25,26] and why the intensity of the rotational excitations was small for hydrogen on Au(110).[7] Local variations of the electrostatic potential, for instance through the Smoluchowski effect[55] in the vicinity of step edges or surface reconstructions, may displace the position of the molecular resonance. The interaction with the metal substrate can furthermore lead to an additional broadening of the molecular resonance and thereby reduce its lifetime with the consequence that an energy transfer from the electron to the inelastic channel becomes inefficient (as was pointed out by W. J. Gadzuk, NIST).

When we take another look at our experimental data, we can extract additional information from the simulations with eq 1 and their approximation to our $d^2I/dV^2$ spectra. First, the RES threshold energies show some variation that can be attributed to subtle compressions of −0.7% and extensions of +1.3% in the bond length with respect to the free molecule.[7] Second, the RES intrinsic peak width ($W_I$, half-width-at-half-maximum) can be related to the lifetime ($\tau$) of the rotationally excited state by $\tau = \hbar/W_I$. The intrinsic width is the residual after accounting for modulation and temperature broadening and frequently approximated *via* $W_I^2 = W_M^2 - W_{mod}^2 - W_T^2$ [5] for inelastic excitations of Lorentzian shape. However, as can be seen from the close-up of the excitations in Figure 3, the Lorentzian is not a good approximation for the resonance enhanced excitations discussed in the present work. We have therefore determined $W_I$ by formally introducing an effective temperature $T_{eff} = T_{STM} + T_\tau$ in the broadening kernel of the above-mentioned convolution (cf. Table 2). The extracted mean lifetimes range from 500 fs to 10 ps. Calculations reported weakly dispersing rotational phonon bands[56] that would broaden the excitation energy implying that the above stated lifetime range represents a lower limit. An upper limit is found when recording *dI/dV* spectra with gradually increasing current. At 500 pA, one electron tunnels every 320 ps, yet we saw no clear sign of pumping into higher lying rotational quantum states. Therefore, the electrons are always probing the molecules in their rotational ground state and the lifetimes of the excited $J = 2$ state are $\tau \ll 320$ ps.

Figure 4 shows an experiment with an isotope mixture of $H_2$, HD, and $D_2$ dosed in the thermodynamic equilibrium concentration of 1:2:1 onto the *h*-BN/Ni(111) surface. The STM image is devoid of any topographic signs for different molecules. Curiously, the *dI/dV* spectrum clearly shows the signatures of all three isotopes with rotational excitations at 22, 31, and 43 meV, corresponding to the known $J = 0 \rightarrow 2$ transitions of the three molecules, and moreover, irrespective of the lateral tip position in the $\sqrt{3}$ structure. The isotopes were shown to not segregate in the first monolayer of the condensed phase and are thereby expected to be randomly distributed.[57] Our findings can consequently be interpreted as RES probing weakly interacting molecular ensembles. We have formerly estimated the ensemble size from the spatial variation of spectra across an *h*-BN-step to be (60 ± 30) molecules.[6]

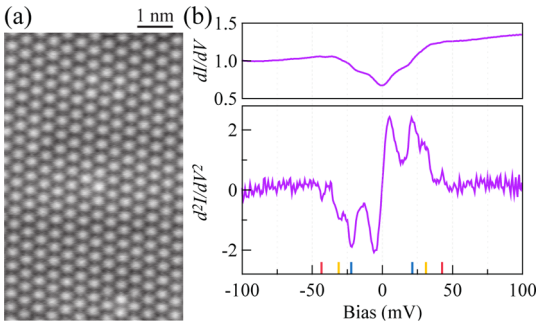


**Figure 4. Ternary mixture of $H_2$, HD, and $D_2$ adsorbed onto *h*-BN/Ni(111) at 10 K. (a) STM image of the mixture showing the $(\sqrt{3} \times \sqrt{3})$R30° superstructure and no apparent height contrast between the three molecular species. (b) The differential conductance spectrum (top) and its numerical derivative show rotational signatures of all three molecules at around 22, 31, and 43 meV ($V_t = -50$ mV, $I_t = 50$ pA, average of 1100 spectra, $R_G = 1$ GΩ).**

It has to be mentioned, however, that the experimental observations for isotopic mixtures can also be reconciled by highly mobile molecules in the $\sqrt{3}$ structure. In this scenario, the molecules would reside mostly in the 6-fold hollow sites and occasionally undergo fast place exchanges. Since STM is a slow technique, the molecules would consequently appear immobile in the $\sqrt{3}$ phase, and the spectra of Figure 4b would correspond to temporal averages of the various molecules with different residence times beneath the tip apex. Although individual hydrogen molecules are highly mobile on graphene and *h*-BN terraces,[57] their mobility ought to be reduced once they condense in the $\sqrt{3}$ phase. If the mobility scenario would apply, a diffusion mechanism with substantial mobility in the $\sqrt{3}$ structure would be required, which awaits further experimental and theoretic scrutiny.

## CONCLUSION

In conclusion, we have shown that STM-RES can be used on a large selection of different substrates. A resonance-mediated tunneling model explains all spectroscopic signatures of hydrogen and of its isotopes. Local variation in the surface potential can lead

to a shift of the molecular resonance position with respect to $E_F$. Since these variations can, in principle, be controlled by external means, the latter example serves as a blueprint for controlling the molecular dynamics of physisorbed molecules. Exploring the resonance mediated tunneling model will furthermore ease the study of alternative molecules that have less pronounced RES transitions, with good starting points proposed in Table 1. It is still an open question whether STM-RES probes ensembles or single molecules.

## METHODS

The measurements were performed with a home-built low-temperature STM operating at 4.7 K and in an ultrahigh vacuum (UHV) chamber with a base pressure of $p_{tot} < 5 \times 10^{-11}$ mbar.[58] We prepared atomically clean single-crystal surfaces of Rh(111), Ni(111), and Ru(0001) by repeated cycles of $Ar^+$ sputtering (10 $\mu$A/cm$^2$, 1 kV, 300 K, 30 min), annealing in oxygen (815 K, 5 min, $2 \times 10^{-7}$ mbar), and flash to 1450, 1100, and 1400 K, respectively. Monolayers of *h*-BN were grown by chemical vapor deposition (CVD) on Ni[31,59,60] and on Rh[37,54,61] at 1040 K with a borazine partial pressure of $2 \times 10^{-6}$ mbar and 3 min exposure. Graphene was either grown by CVD on Ni[28] at 800 K or on Ru[62,63] at 1000 K, using an ethylene partial pressure of $1 \times 10^{-6}$ mbar for 10 min, or it was prepared by simply heating a Ru crystal to 1200 K that had experienced several CVD cycles before.[64,63] Subsequent to the layer growth, the samples were cooled to 10 K and exposed to hydrogen. We dosed molecular hydrogen, deuterium, and a mixture of both by backfilling the UHV chamber through a leak-valve. The $H_2-HD-D_2$ mixture was heated to 500 K in a dedicated volume in order to accelerate the transition into the thermodynamic equilibrium with a well-defined $H_2/HD/D_2$ ratio of 1:2:1. Note that all pressure values state the readout of a $N_2$-calibrated ionization gauge. The STM images were acquired at constant current, and the indicated tunnel voltages ($V_t$) correspond to the sample potential (cf. Figure 1). Scanning tunneling spectroscopy was performed by recording the bias-dependent differential conductance (*dI*/*dV*) using a lock-in amplifier and adding a sinusoidal 2 mV peak-to-peak modulation at 397 Hz to the bias voltage. For every point spectrum, the tip was first stabilized at negative bias with $R_G = 1$ GΩ, the feedback loop was then opened, and a single *dI*/*dV* curve was recorded within 40 s. Both, electrochemically etched tungsten and wire-cut platinum–iridium tips were used for spectroscopy without yielding significant differences in the spectral line-shapes. Tip conditioning steps included sputtering in UHV before the transfer into the STM, voltage pulses, and occasional gentle poking into the surface. In figures showing more than one *dI*/*dV* curve, the upper spectra were offset by one unit for clarity. $d^2I/dV^2$ curves were obtained numerically with the central difference method from experimental *dI*/*dV* data. The simulations with eq 1 were carried out as follows: (1) An initial trial function was calculated for *dI*/*dV* with eq 1 and the numerically differentiated function brought to a close match with experimental $d^2I/dV^2$ data in order to quickly curtail the parameter space. (2) A new trial function was then numerically convolved with the common broadening kernel accounting for temperature and modulation.[4,52] (3) The convolved curve was numerically differentiated and compared with experimental $d^2I/dV^2$ curves. (4) The free parameters and the effective temperature were varied and steps 2 and 3 repeated. (5) The quality of the simulation was finally gauged with the sum of squared residuals.

*Conflict of Interest:* The authors declare no competing financial interest.

*Acknowledgment.* We gratefully acknowledge funding from the Swiss National Science Foundation (SNSF). F.D.N. also acknowledges financial support from SNSF Early Postdoc.Mobility fellowship under project number 148891 and fruitful discussions with W. J. Gadzuk, NIST.

## REFERENCES AND NOTES

1. Heisenberg, W. Mehrkörperprobleme und Resonanz in der Quantenmechanik. II. *Z. Phys.* **1927**, *41*, 239–267.
2. Bonhoeffer, K. F.; Harteck, P. Para- and Ortho Hydrogen. *Z. Phys. Chem. B* **1929**, *4*, 113–141.
3. A comprehensive database of rotational constants for various molecules: http://cccbdb.nist.gov/, accessed 07/07/2014.
4. Lambe, J.; Jaklevic, R. C. Molecular Vibration Spectra by Inelastic Electron Tunneling. *Phys. Rev.* **1968**, *165*, 821–832.
5. Wolf, E. L. *Principles of Electron Tunneling Spectroscopy*, 2nd ed.; Oxford University Press: New York, 2012.
6. Natterer, F. D.; Patthey, F.; Brune, H. Distinction of Nuclear Spin States with the Scanning Tunneling Microscope. *Phys. Rev. Lett.* **2013**, *111*, 175303.
7. Li, S.; Yu, A.; Toledo, F.; Han, Z.; Wang, H.; He, H. Y.; Wu, R.; Ho, W. Rotational and Vibrational Excitations of a Hydrogen Molecule Trapped within a Nanocavity of Tunable Dimension. *Phys. Rev. Lett.* **2013**, *111*, 146102.
8. Stipe, B. C.; Rezaei, M. A.; Ho, W. Single Molecule Vibrational Spectroscopy and Microscopy. *Science* **1998**, *280*, 1732–1735.
9. Lauhon, L. J.; Ho, W. Single-molecule Vibrational Spectroscopy and Microscopy: CO on Cu(001) and Cu(110). *Phys. Rev. B* **1999**, *60*, R8525.
10. Stipe, B. C.; Rezaei, M. A.; Ho, W. Coupling of Vibrational Excitation to the Rotational Motion of a Single Adsorbed Molecule. *Phys. Rev. Lett.* **1998**, *81*, 1263–1266.
11. Heinrich, A. J.; Gupta, J. A.; Lutz, C. P.; Eigler, D. M. Single-Atom Spin-Flip Spectroscopy. *Science* **2004**, *306*, 466–469.
12. Otte, A. F.; Ternes, M.; Bergmann, K. v.; Loth, S.; Brune, H.; Lutz, C. P.; Hirjibehedin, C. F.; Heinrich, A. J. The Role of Magnetic Anisotropy in the Kondo Effect. *Nat. Phys.* **2008**, *4*, 847–850.
13. Khajetoorians, A. A.; Lounis, S.; Chilian, B.; Costa, A. T.; Zhou, L.; Mills, D. L.; Wiebe, J.; Wiesendanger, R. Itinerant Nature of Atom-Magnetization Excitation by Tunneling Electrons. *Phys. Rev. Lett.* **2011**, *106*, 037205.
14. Donati, F.; Dubout, Q.; Autès, G.; Patthey, F.; Calleja, F.; Gambardella, P.; Yazyev, O. V.; Brune, H. Magnetic Moment and Anisotropy of Individual Co Atoms on Graphene. *Phys. Rev. Lett.* **2013**, *111*, 236801.
15. Nielsen, M.; McTague, J. P.; Ellenson, W. Adsorbed Layers of $D_2$, $H_2$, $O_2$, and $^3He$ on Graphite Studied by Neutron Scattering. *J. Phys., Colloq.* **1977**, *38*, C4–10-C4–18.
16. Frank, V. L. P.; Lauter, H. J.; Leiderer, P. Phonons in the Commensurate Monolayer of $D_2$ on Graphite. *Phys. Rev. Lett.* **1988**, *61*, 436–439.
17. Kubik, P. R.; Hardy, W. N.; Glattli, H. Orientational Ordering of Hydrogen Molecules Adsorbed on Graphite. *Can. J. Phys.* **1985**, *63*, 605–620.
18. Kim, K.; Sullivan, N. S. Orientational Behavior of Quantum Rotors Physisorbed on Boron Nitride. *Phys. Rev. B* **1997**, *55*, R664–R667.
19. Andersson, S.; Harris, J. Observation of Rotational Transitions for $H_2$, $D_2$, and HD Adsorbed on Cu(100). *Phys. Rev. Lett.* **1982**, *48*, 545–548.
20. Avouris, P.; Schmeisser, D.; Demuth, J. E. Observation of Rotational Excitations of $H_2$ Adsorbed on Ag Surfaces. *Phys. Rev. Lett.* **1982**, *48*, 199–202.
21. Palmer, R.; Willis, R. Rotational States of Physisorbed Hydrogen on Graphite. *Surf. Sci.* **1987**, *179*, L1–L5.
22. Traeger, F.; Toennies, J. P. Helium Atom Scattering Studies of the Structures and Vibrations of the $H_2$, HD, and $D_2$ Monolayers on NaCl(001). *J. Phys. Chem. B* **2004**, *108*, 14710–14725.
23. Persson, B. N. J.; Baratoff, A. Inelastic Electron Tunneling from a Metal Tip: The Contribution from Resonant Processes. *Phys. Rev. Lett.* **1987**, *59*, 339–342.

24. Baratoff, A.; Persson, B. N. J. Theory of the Local Tunneling Spectrum of a Vibrating Adsorbate. *J. Vac. Sci. Technol. A* **1988**, *6*, 331–335.
25. Gupta, J. A.; Lutz, C. P.; Heinrich, A. J.; Eigler, D. M. Strongly Coverage-Dependent Excitations of Adsorbed Molecular Hydrogen. *Phys. Rev. B* **2005**, *71*, 115416.
26. Temirov, R.; Soubatch, S.; Neucheva, O.; Lassise, A. C.; Tautz, F. S. A Novel Method Achieving Ultra-High Geometrical Resolution in Scanning Tunnelling Microscopy. *New J. Phys.* **2008**, *10*, 053012.
27. Weiss, C.; Wagner, C.; Kleimann, C.; Tautz, M. R. F. S.; Temirov, R. Imaging Pauli Repulsion in Scanning Tunneling Microscopy. *Phys. Rev. Lett.* **2010**, *105*, 086103.
28. Gamo, Y.; Nagashima, A.; Wakabayashi, M.; Terai, M.; Oshima, C. Atomic Structure of Monolayer Graphite Formed on Ni(111). *Surf. Sci.* **1997**, *347*, 61–64.
29. Auwärter, W.; Kreutz, T. J.; Greber, T.; Osterwalder, J. XPD and STM Investigation of Hexagonal Boron Nitride on Ni(111). *Surf. Sci.* **1999**, *429*, 229–236.
30. Grad, G. B.; Blaha, P.; Schwarz, K.; Auwärter, W.; Greber, T. Density Functional Theory Investigation of the Geometric and Spintronic Structure of h-BN/Ni(111) in View of Photoemission and STM Experiments. *Phys. Rev. B* **2003**, *68*, 085404.
31. Preobrajenski, A. B.; Vinogradov, A. S.; Mårtensson, N. Ni 3d-BN Hybridization at the h-BN Ni(111) Interface Observed with Core-Level Spectroscopies. *Phys. Rev. B* **2004**, *70*, 165404.
32. Seguin, J. L.; Suzanne, J. A LEED Study of Physisorbed Hydrogen on Graphite. *Surf. Sci.* **1982**, *118*, L241–L245.
33. Kim, K.; Sullivan, N. Orientational Ordering in Monolayer Films of Molecular Hydrogen on Boron Nitride. *J. Low Temp. Phys.* **1999**, *114*, 173–201.
34. Martoccia, D.; Willmott, P. R.; Brugger, T.; Björck, M.; Günther, S.; Schlepütz, C. M.; Cervellino, A.; Pauli, S. A.; Patterson, B. D.; Marchini, S.; Wintterlin, J.; Moritz, W.; Greber, T. Graphene on Ru(0001): A 25 × 25 Supercell. *Phys. Rev. Lett.* **2008**, *101*, 126102.
35. Iannuzzi, M.; Kalichava, I.; Ma, H.; Leake, S. J.; Zhou, H.; Li, G.; Zhang, Y.; Bunk, O.; Gao, H.; Hutter, J.; Willmott, P. R.; Greber, T. Moiré Beatings in Graphene on Ru(0001). *Phys. Rev. B* **2013**, *88*, 125433.
36. Ding, Y.; Iannuzzi, M.; Hutter, J. Investigation of Boron Nitride Nanomesh Interacting with Water. *J. Phys. Chem. C* **2011**, *115*, 13685–13692.
37. Corso, M.; Auwärter, W.; Muntwiler, M.; Tamai, A.; Greber, T.; Osterwalder, J. Boron Nitride Nanomesh. *Science* **2004**, *303*, 217–220.
38. Bunk, O.; Corso, M.; Martoccia, D.; Herger, R.; Willmott, P. R.; Patterson, B. D.; Osterwalder, J.; Veen, J. F. v. d.; Greber, T. Surface X-ray Diffraction Study of Boron-Nitride Nanomesh in Air. *Surf. Sci.* **2007**, *601*, L7–L10.
39. Laskowski, R.; Blaha, P.; Gallauner, T.; Schwarz, K. H. Single-Layer Model of the Hexagonal Boron Nitride Nanomesh on the Rh(111) Surface. *Phys. Rev. Lett.* **2007**, *98*, 106802.
40. Ilisca, E. Ortho-Para Conversion of Hydrogen Molecules Physisorbed on Surfaces. *Prog. Surf. Sci.* **1992**, *41*, 217–335.
41. Ilisca, E. Hydrogen Conversion on Nonmagnetic Insulating Surfaces. *Europhys. Lett.* **2013**, *104*, 18001.
42. Bedrossian, P.; Chen, D. M.; Mortensen, K.; Golovchenko, J. A. Demonstration of the Tunnel-Diode Effect on an Atomic Scale. *Nature* **1989**, *342*, 258–260.
43. Lyo, I. W.; Avouris, P. Negative Differential Resistance on the Atomic Scale: Implications for Atomic Scale Devices. *Science* **1989**, *245*, 1369–1371.
44. Fano, U. Effects of Configuration Interaction on Intensities and Phase Shifts. *Phys. Rev.* **1961**, *124*, 1866–1878.
45. Gaudioso, J.; Lauhon, L. J.; Ho, W. Vibratiolly Mediated Negative Differential Resistance in a Single Molecule. *Phys. Rev. Lett.* **2000**, *85*, 1918–1921.
46. Halbritter, A.; Makk, P.; Csonka, S.; Mihály, G. Huge Negative Differential Conductance in Au-$H_2$ Molecular Nanojunctions. *Phys. Rev. B* **2008**, *77*, 075402.
47. Smit, R. H. M.; Noat, Y.; Untiedt, C.; Lang, N. D.; van Hemert, M. C.; van Ruitenbeek, J. M. Measurement of the Conductance of a Hydrogen Molecule. *Nature* **2002**, *419*, 906–909.
48. Thijssen, W. H. A.; Djukic, D.; Otte, A. F.; Bremmer, R. H.; van Ruitenbeek, J. M. Vibrationally Induced Two-Level Systems in Single-Molecule Junctions. *Phys. Rev. Lett.* **2006**, *97*, 226806.
49. Schulz, G. J. Resonances in Electron Impact on Diatomic Molecules. *Rev. Mod. Phys.* **1973**, *45*, 423–486.
50. Palmer, R. E.; Rous, P. J. Resonances in Electron Scattering by Molecules on Surfaces. *Rev. Mod. Phys.* **1992**, *64*, 383–440.
51. Teillet-Billy, D.; Gauyacq, J. P.; Persson, M. Molecular Rotation Induced by Inelastic Electron Tunneling. *Phys. Rev. B* **2000**, *62*, R13306.
52. Klein, J.; Léger, A.; Belin, M.; Défourneau, D.; Sangster, M. J. L. Inelastic-Electron-Tunneling Spectroscopy of Metal-Insulator-Metal Junctions. *Phys. Rev. B* **1973**, *7*, 2336–2348.
53. Dil, H.; Lobo-Checa, J.; Laskowski, R.; Blaha, P.; Berner, S.; Osterwalder, J.; Greber, T. Surface Trapping of Atoms and Molecules with Dipole Rings. *Science* **2008**, *319*, 1824–1826.
54. Natterer, F. D.; Patthey, F.; Brune, H. Ring State for Single Transition Metal Atoms on Boron Nitride on Rh(111). *Phys. Rev. Lett.* **2012**, *109*, 066101.
55. Smoluchowski, R. Anisotropy of the Electronic Work Function of Metals. *Phys. Rev.* **1941**, *60*, 661–674.
56. Janssen, W. B. J. M.; Berg, T. H. M. d.; Avoird, A. v. d. Phonons and Rotons in Commensurate p-$H_2$ and o-$D_2$ Monolayers on Graphite. *Phys. Rev. B* **1991**, *43*, 5329–5337.
57. Bienfait, M.; Zeppenfeld, P.; Ramos, R. C.; Gay, J. M.; Vilches, O. E.; Coddens, G. Isotopic Ordering in Adsorbed Hydrogen Monolayers. *Phys. Rev. B* **1999**, *60*, 11773.
58. Gaisch, R.; Gimzewski, J. K.; Reihl, B.; Schlittler, R. R.; Tschudy, M.; Schneider, W. D. Low-Temperature Ultra-High Vacuum Scanning Tunneling Microscope. *Ultramicroscopy* **1992**, *42*, 1621–1626.
59. Nagashima, A.; Tejima, N.; Gamou, Y.; Terai, M.; Oshima, C. Electronic Dispersion Relations of Monolayer Hexagonal Boron Nitride formed on the Ni(111) Surface. *Phys. Rev. B* **1995**, *51*, 4606–4613.
60. Natterer, F. D.; Patthey, F.; Brune, H. Quantifying Residual Hydrogen Adsorption in Low-Temperature STMs. *Surf. Sci.* **2013**, *615*, 80–87.
61. Preobrajenski, A. B.; Vinogradov, A. S.; Ng, M. L.; Cavar, E.; Westerstrom, R.; Mikkelsen, A.; Lundgren, E.; Mårtensson, N. Influence of Chemical Interaction at the Lattice-Mismatched h-BN/Rh(111) and h-BN/Pt(111) Interfaces on the Overlayer Morphology. *Phys. Rev. B* **2007**, *75*, 245412.
62. Loginova, E.; Bartelt, M. C.; Feibelman, P. J.; McCarty, K. F. Factors Influencing Graphene Growth on Metal Surfaces. *N. J. Phys.* **2009**, *11*, 063046.
63. Natterer, F. D.; Rusponi, S.; Papagno, M.; Carbone, C.; Brune, H. Optimizing Long-range Order, Band Gap, and Group Velocities for Graphene on close-packed metal surfaces. *J. Phys.: Condens. Matter* **2012**, *24*, 314203.
64. Sutter, P. W.; Flege, J. I.; Sutter, E. A. Epitaxial Graphene on Ruthenium. *Nat. Mater.* **2008**, *7*, 406–411.